Pseudorange Measurements with LTE Physical Channels

Auryn P. Soderini, Paul Thevenon, Christophe Macabiau, *ENAC, Université de Toulouse*
Laurent Borgagni, John Fischer, *Orolia*

BIOGRAPHIES

Auryn Soderini is a Ph.D. student in the Department of Air Navigation Engineering and Science at the French National School of Civil Aviation, Toulouse, France. He received his M.Sc. degrees from Tampere University of Technology, Finland, in 2016. He is a member of the Signal Processing and Navigation research group. His current research interests focus on signal processing for positioning and navigation in mobile networks.

Paul Thevenon graduated as electronic engineer from Ecole Centrale de Lille in 2004 and obtained in 2007 a research master at ISAE in space telecommunications. In 2010, he obtained a PhD degree in the signal processing laboratory of ENAC in Toulouse, France. From 2010 to 2013, he was employed by CNES, the French space agency, to supervise GNSS research activities and measurement campaigns. Since the July 2013, he is employed by ENAC as Assistant Professor. His current activities are GNSS signal processing, GNSS integrity monitoring and hybridization of GNSS with other sensors.

Christophe Macabiau graduated as electronics engineer in 1992 from the ENAC in Toulouse, France. Since 1994, he has been working on the application of satellite navigation techniques to civil aviation. He received his Ph.D in 1997 and has been in charge of the signal processing lab of ENAC from 2000 to 2012. He is currently the head of the TELECOM team of ENAC.

Laurent Borgagni is a Research and Development Director and John Fischer is an Advanced Research and Development Vice President at Orolia, a world leader in GPS-based time and frequency equipment.

ABSTRACT

The long-term evolution (LTE) reference signals, such as the primary synchronization signal (PSS), secondary synchronization signal (SSS) and cell-specific reference signal (CRS), have been studied for navigation. The signal structure including its influence on signal tracking has been previously discussed. However, there are non-reference signals such as the physical broadcast channel (PBCH), physical control format indicator channel (PCFICH), physical hybrid automatic repeat request (HARQ) indicator channel (PHICH) and physical downlink control channel (PDCCH) that can also be used for navigation. To the authors' knowledge, pseudorange estimates with LTE physical channels have been almost not considered in the literature. This paper makes two contributions. First, the LTE physical channels properties which are relevant for signal tracking are discussed. Second, the expected tracking performance with LTE physical channels used in a standalone fashion are evaluated.

1 INTRODUCTION

In urban areas, buildings, trees and other elements such as interference and spoofing can reduce the performance of navigation systems exclusively based on global navigation satellite systems (GNSS). A common approach to tackle performing limitations of GNSS-based navigation uses aiding sensors, including inertial sensors, vision sensors and laser sensors; and also map matching algorithms [1, 2].

In the recent years, alternative navigation solutions using ambient signals from several diverse sources including radio cellular networks, television/radio broadcast networks, wireless local area networks and satellite communication networks have been approached [3-8]. Among these ambient signals, long-term evolution (LTE) signals are particularly attractive because have high bandwidth and high received power; moreover, they are almost ubiquitous in urban situations.

A communication receiver with built-in functions such as time synchronization and channel estimation measuring received signal time delay can further be completed by additional functions to meet demanding positioning accuracy requirements. Extracting time delay information is seen as the natural way to address localization opportunistically, although other ways using different metrics such as angle of arrival, not primarily focused in this paper, may be pursued.

Several reference signals in LTE, such as the primary synchronization signal (PSS), secondary synchronization signal (SSS) and cell-specific reference signal (CRS), have been studied for navigation. The structure for such signals and its influence on signal tracking has been discussed in [8]. It has been demonstrated that the CRS can offer much better performance than the

PSS and SSS can do. Besides, there are other signals in LTE that can be used for navigation which have been almost not considered in literature.

In this paper, the potentials of the physical channels (PHYCHs) in LTE systems for ranging estimation accuracy are evaluated.

The first section of this paper is an introduction. Section 2 describes the LTE physical channels properties which are relevant for signal tracking. Section 3 describes the autocorrelation function properties for the LTE physical channels and discusses the signal tracking error variance due to the channel additive white noise. Section 4 demonstrates the signal tracking performance for the different physical channels comparatively. Finally, Section 5 draws the conclusions and identifies the future work.

2 LTE PHYCH PROPERTIES FOR SIGNAL TRACKING

2.1 Frame structure

Orthogonal frequency division multiplexing (OFDM) is used in LTE systems to encode the downlink data. In such multicarrier transmission scheme, the channel bandwidth W is divided into several narrow and equally spaced sub-bands referred to as subcarriers. Ideally, the maximum of each subcarrier spectrum is located at the zero-crossing frequency of the remaining subcarriers. Thus, the subcarriers spectrum to some extent overlaps to each other while not produce interference. Hence, the spectrum efficiency is increased. The spectrum orthogonality and other properties associated with the subcarriers in OFDM signals are discussed in [8].

In OFDM digital transmissions, the inverse fast Fourier transform (IFFT) algorithm is used at the transmitter to encode data symbol blocks to OFDM symbols; and the fast Fourier transform (FFT) algorithm is used at the receiver to decode OFDM symbols to data symbol blocks. These algorithms since having low complexity can support as many inputs/outputs as required in LTE systems for the encoding and the decoding operations schematized in Figure 1. In LTE systems, the total number of subcarriers N_c and the number of subcarriers that can carry data N_d in an OFDM symbol can be assigned by the network provider to the values presented in Table 1.

The LTE systems use the cyclic prefix (CP) sequence, which is a copy of the terminal portion of the OFDM symbol appended at the OFDM symbol front. This allows to increase the overall symbol duration (at the expense of data rate) with no need to reduce the subcarrier spacing, which is appropriate to reduce inter-symbol interference due to multipath while keeping synchronization error sensitivity unchanged; and it makes the OFDM symbol demodulation robust to the OFDM symbol start synchronization errors.

The OFDM signal bandwidth, which consists of N_c subcarriers, is defined as equal to the sampling frequency F_s. Thus, the sampling frequency divided by the total number of subcarriers returns the subcarriers spacing Δ_c, which is the frequency resolution of subchannels, typically 15 kHz in an LTE system. Likewise, the sampling interval T_s multiplied by the total number of subcarriers returns the duration of the OFDM symbols Δ_s (without cyclic prefix).

In LTE systems based on the frequency division duplexing (FDD) transmission type, the downlink signal structure is organized in frames, subframes and slots; where each frame (10 ms) can be decomposed into 10 subframes and each subframe (1 ms) can be decomposed into 2 slots (0.5 ms). Then, a slot can be decomposed in multiple resource blocks (RBs), which denote the minimum amount of transmission resources that can be allocated to the user equipment (UE) in a time slot. For normal CP, an RB consists of 12 subcarriers and 7 OFDM symbols. The total number of downlink resource blocks N_{RB}^{DL} per slot increases as a function of the deployed channel bandwidth. Lastly, an RB can be decomposed in multiple resource elements (REs), which are the smallest elements of the frame that can be associated with subcarriers and OFDM symbols. Note that the OFDM symbols in each subframe are numbered from 0 to 13. The LTE frame structure is illustrated in Figure 2.

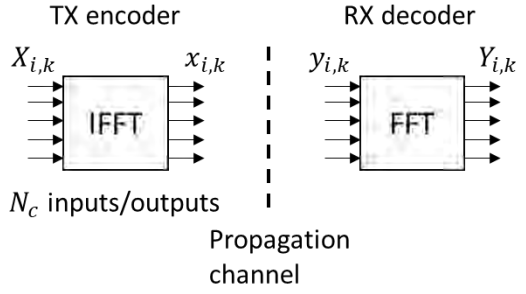

Figure 1. OFDM encoding and decoding blocks. Notation: $X_{i,k}$, TX data symbols; $x_{i,k}$, TX OFDM symbols; $y_{i,k}$, RX OFDM symbols; $Y_{i,k}$, RX data symbols. The letters i and k represent the OFDM symbol index and the subcarrier index, respectively. Abbreviations: TX, transmitter; RX, receiver

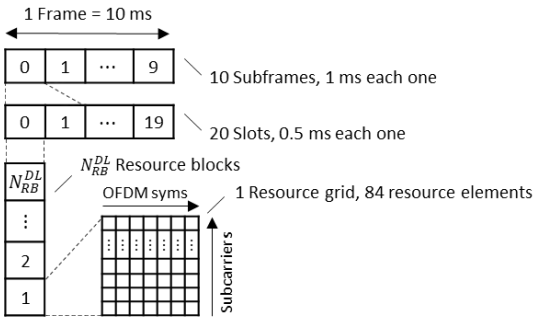

Figure 2. LTE frame structure. Abbreviation: syms, symbols

Table 1. LTE DL modulation main parameters

W [MHz]	N_{RB}^{DL}	N_c	N_d	F_s [MHz]
1.4	6	128	72	1.92
3	15	256	180	3.84
5	25	512	300	7.68
10	50	1024	600	15.36
15	75	1536	900	23.04
20	100	2048	1200	30.72

2.2 Physical channels

A downlink physical channel is a set of resource elements associated with frequency and time that carries higher layers originated information, referred to as codeword. This data also known as transport block undergoes the physical channel processing chain [9, 10] before being transmitted on a physical channel in the form of baseband data. The baseband data for a downlink physical channel is defined through the steps in Figure 3. First, coded bits in each of the codewords being transmitted on a physical channel are scrambled. Second, scrambled bits are modulated to generate complex-valued modulation symbols. Third, complex-valued modulation symbols are mapped onto one or several transmission layers. Fourth, complex-valued modulation symbols on each layer are pre-coded for transmission on the antenna ports. Last, complex-valued modulation symbols for each antenna port are mapped to resource elements with which the OFDM signal is generated.

The physical channels that can be approached for signal tracking are listed as follows: physical broadcast channel (PBCH), physical control format indicator channel (PCFICH), physical hybrid automatic repeat request (HARQ) indicator channel (PHICH), and physical downlink control channel (PDCCH). In this paper, the PBCH, PCFICH, and PHICH are considered; the PDCCH will be addressed in a separate work.

The PHYCH data symbols are associated with a digital modulation scheme of either second or fourth order (defined as the symbol alphabet size) depending on the channel being examined. Each PHYCH data symbol, therefore, corresponds to either one or two bits. PHYCHs are meant to provide low data rate and high robust symbol detection transmissions and, as such, can be replicated reliably at the receiver for correlation and delay estimation purposes.

The payload data which is carried by the physical downlink shared channel (PDSCH) is associated, instead, with a modulation order often higher than fourth, which can be two hundred fifty-sixth at the most; that is an accordingly higher number of bits per symbol. For this reason, the PDSCH is considered less attractive than the remaining physical channels can be.

In LTE, the cyclic prefix can be either normal or extended [9]. In what follows, it is assumed the normal CP unless being the contrary explicitly said. The aim is to reduce the technical complexity of the topic while facilitating the understanding of proof concept.

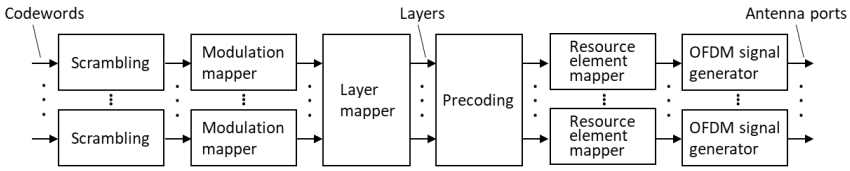

Figure 3. LTE downlink physical channel processing chain

PBCH

The physical broadcast channel carries exclusively the master information block (MIB), which is a transport block (bits) coding system information, such as the system bandwidth, PHICH configuration (made up of two informative components, namely: PHICH resource indicator and PHICH duration) and system frame number (SFN). The latter is a periodic sequence (0-1023) with which radio frames are numbered. The MIB codeword after scrambling corresponds uniquely to the physical layer cell identity (PCI).

At the receiver, the system bandwidth and the SFN are acquired after PBCH passing through the backward physical channel processing chain [9-11]. Once acquired, the MIB can be reproduced. Then, the receiver can perform PBCH tracking without the constraint of PBCH decoding. This allows the receiver to perform signal tracking at signal to noise ratio below the communication requirement, which means that the receiver does not necessarily need to be within the coverage area of the serving base station.

The PBCH data symbols are mapped to specific resource elements and can be decoded 25 times per second in nominal communication system conditions, which is a useful rate for getting pseudorange measurements. In details, the entire sequence (960 data symbols) is mapped across four consecutive frames (240 data symbols per frame), as of any frame whose identification number divided by four returns null remainder; one fourth of the sequence in each frame is mapped across four OFDM symbols in the subframe number zero, specifically, OFDM symbol number (OSN) 7 to 10; each sequence quarter repeats every four frames (40 ms).

The PBCH data symbols are mapped within the central 72 resource elements of the system bandwidth. The specific subcarrier allocation is illustrated in Figure 4 with an example. The number of PBCH data symbols differ from OSNs 7, 8 (48 subcarriers) to OSNs 9, 10 (72 subcarriers). In OSNs 7, 8 a reduced number of PBCH data symbols are carried, notably at frequencies not occupied with CRS reference symbols. In this paper, we will use the term PBCH-48 to indicate either the PBCH in OSN 7 or the PBCH in OSN 8; likewise, we will use the term PBCH-72 to indicate either the PBCH in OSN 9 or the PBCH in OSN 10.

For PBCH, the quadrature phase shift keying (QPSK) modulation is used to ease the demodulation of such low data rate channel. A limitation of PBCH in LTE systems is represented by its relatively small bandwidth (1 MHz) which is constant regardless from the used system bandwidth.

Figure 4. An example of data symbols allocated within the central 72 resource elements of the system bandwidth to antenna port number zero with two antenna ports configuration

PCFICH

The physical control format indicator channel carries the control format indicator (CFI) denoting the number of OFDM symbols (up to 3) that are used for the transmission of the PDCCH in subframe number zero. The CFI represents an integer number among three options (1, 2 or 3), which maps to a codeword (31-bits) with the matching rule in [10]. The CFI assignation is dependent upon the system bandwidth and user equipment category which are constant for a given system configuration. The CFI codewords are scrambled with pseudo-random codes associated with two parameters, namely the physical layer cell identity and the slot number (n_s). Scrambling of the CFI codewords allows to eliminate interference from other cell transmissions which appear as uncorrelated noise at the receiver after the received bit stream is descrambled. The number of bits in a CFI scrambled codeword (32 bits) is not dependent upon the CFI and hence after the QPSK modulation also the number of PCFICH data symbols (16 data symbols) in an OFDM symbol is not dependent upon the CFI. The PCFICH sequence length does not change with any of the following parameters: PCI, SFN and N_{RB}^{DL}.

The PCFICH structure occupies four resource element groups (REGs), where REG is a resource allocation unit with four consecutive resource elements not including those being used by the reference signals.

The PCFICH REGs are located evenly across almost the whole channel bandwidth. The PCFICH REG locations are dependent upon N_{RB}^{DL} and PCI. In details, the PCFICH REG locations expand (and hence the REG spacing increases) over a wider bandwidth with N_{RB}^{DL}; and such locations shift of a common offset as a function of the PCI with a mechanism that reduces the intra-band interference. Finally, the PCFICH REG locations are not dependent upon the SFN number.

PHICH

The physical hybrid automatic repeat request (HARQ) indicator channel carries the HARQ indicator (HI) for the downlink transmission of acknowledgement (ACK) and negative acknowledgement (NACK), signaling on whether a physical uplink shared channel (PUSCH) transmission has been received, and hence a method for determining whether the uplink retransmission of a transport block for error correction is required.

The PHICH duration, which is carried in the MIB informative block can be either normal or extended. In this paper, we consider the normal PHICH duration (PHICH is located only in the OFDM symbol number zero), as it is the typical scenario. For clarity, it is assumed always the normal PHICH duration even when not explicitly said.

At the transmitter, the HI (1 bit) indicator is repeated three times for error correction coding forming the HI codeword (3 bits). The HI codeword after the binary phase shift keying (BPSK) modulation is turned into a block of three complex symbols. Therein, each symbol is repeated four times for redundant detection and each of the repeated sequences is multiplied, firstly, to an orthogonal sequence for PHICH multiplexing and, secondly, to a pseudo-random sequence for rejection of inter-cell interference. After that, the sequence associated with HI is made up 12 data symbols. The PHICH multiplexing is correspondent to a sum operation of orthogonal sequences not affecting the multiplexed sequence length.

The HI indicator depends upon uplink data reception which is relative to the UE location and dynamics. Thus, the PHICH changes in time with the SFN. For this reason, the PHICH demodulation cannot be bypassed using a prerecorded information. Indeed, PHICH tracking requires a punctual replication of the signal. This relationship of dependence between the communication system and the signal tracking system, in which PHICH tracking is subject to PHICH being demodulated, is generally not desired. However, the BPSK modulation is much robust to the signal degradation due to noise. Therefore, the requirement of PHICH demodulation is not considered an issue.

In general terms, the PHICH structure occupies a plurality of PHICH groups in the OFDM symbol number zero wherein each PHICH group occupies three REGs across most of the channel bandwidth. Thus, the number of PHICH resource elements in an OFDM symbol is correspondent to an integer multiple of three REG groups. Each PHICH group can carry at least a PHICH sequence, and up to eight PHICH sequences can be multiplexed within each PHICH group for the transmission of separate HARQ ACK/NACK signals. The PHICH is transmitted in each SFN at the rate of thousand times per second.

The number of PHICH groups in a subframe can be assigned by the network provider to the values in Equation (1) [9],

$$N_{PHICH}^{\text{group}} = \left\lceil N_g \, N_{RB}^{DL} / 8 \right\rceil \tag{1}$$

where $\lceil x \rceil$ is the ceiling function which maps x to the smallest integer greater than or equal to x; $N_g = \{1/6, 0.5, 1, 2\}$, which is carried by the PBCH physical channel and is called PHICH resource indicator, is the scale factor between the reference number and the corresponding configuration number of PHICH REs which are dependent to N_{RB}^{DL}.

The PHICH configuration does not change with the SFN number. However, several PHICH REs may carry no data depending on the network load. In fact, as the number of UEs drops so does the associated signaling load.

The three PHICH REGs in each PHICH group are located almost evenly across most of the channel bandwidth. The PHICH REG locations are variant with N_g, N_{RB}^{DL} and PCI. The PHICH REG locations expand over a wider bandwidth with N_{RB}^{DL}, and they shift with a common offset, which is ruled by the PCI, plus an individual smaller offset which serve to fit them into the available resources.

In summary, firstly, the PHICH structure changes (in terms of total number of subcarriers and subcarriers allocation) with N_g and N_{RB}^{DL} and, secondly, the PCI does not affect the PHICH structure although it changes its frequency offset.

3 LTE PHYCH EXPECTED TRACKING PERFORMANCE

3.1 Autocorrelation amplitude characterization

CIR estimation

It is shown in [8] that the normalized channel impulse response (CIR) can be estimated with respect to the i-th OFDM symbol by correlating the received pilots and a local replica of the transmitted pilots, the latter modelled as transmitted data symbols (whose values are known) for a frequency index within the pilot frequency index space and zeros elsewhere. Furthermore, it is shown that such estimate, for a relatively small offset between the correlation delay and the propagation delay of the received signal, can be approximated as

$$\tilde{h}_{i,\epsilon} = \sigma_{p_i}^2 a_{i,\epsilon} \operatorname{sinc} \pi\beta\epsilon + v_{i,\epsilon} \tag{2}$$

with the notation summarized as follows:

$\sigma_{p_i}^2$ is the power of the transmitted pilots of the i-th OFDM symbol
$a_{i,\epsilon}$ reflects the amplitude attenuation and phase rotation of the direct propagation component of the single-path channel relative to the i-th OFDM symbol
β is a positive constant which is related to the structure of the pilot symbols
$\epsilon = \tau - \hat{\tau}$, with τ the normalized propagation delay at the time of synchronizing the residual timing error; and with $\hat{\tau}$ the τ estimate; ϵ denotes the normalized residual timing error
$v_{i,\epsilon}$ denotes the correlation of the local replica of the transmitted pilots with the channel noise with respect to the i-th OFDM symbol

The Equation (2) is valid under the assumption that the received data symbols at the receiver FFT input are perfectly frequency synchronized. In addition, the propagation channel includes only the direct path and adds a complex white noise to each data symbol. A complex white noise, as such, is modelled as a zero-mean Gaussian random variable.

PBCH ACF individual analysis

The autocorrelation function (ACF) amplitude associated with PBCH-48 and the ACF amplitude associated with PBCH-72 are illustrated in Figure 5. The two shapes, which for a small correlation delay are sine cardinalis functions, are proportional to each other. The relative amplitude of the two shapes is a scale factor of 1.5. The sine cardinalis shape associated with PBCH-48 (blue line) exhibits a copy of itself (scaled by a factor 0.5) on both sides and at large distance (±6651 m) from the synchronization point. Its maximum value at the origin of correlation delay axis is equal to 48. The sine cardinalis shape associated with PBCH-72 (red line) shows a maximum value equal to 72. The main lobe of the two shapes is as much wide as 562 m. The maximum value and the width of the main lobe of the two shapes are illustrated in Figure 6.

There are situations where, if the acquisition delay error exceeds the main lobe width, the side lobes of the sine cardinalis function could help the delay tracking to converge towards the main lobe, depending on system dynamics and tracking parameters. However, there are many situations in which the side lobes of the autocorrelation function under large acquisition errors lead to biased delay tracking estimates. It is also possible that the delay tracking jumps from one side lobe to another one randomly. In general, if the estimation bias due to the multiple peaks cannot be resolved, and not even bounded, then the ACF side lobes may not be desired.

The threat posed by the second order main lobes associated with PBCH-48 is quite much significant for the following reasons. First, the second order main lobe is relatively high which enhance the possibility of biased delay being tracked in presence of thermal noise. Then, the second order main lobe is located far away from the delay origin and hence associated with large estimation bias. Last, the side lobes associated with the second order main lobe could lead the delay tracking to converge towards largely biased estimates.

There is a scale factor of 4.6 between the height of the main lobe and the height of the first side lobe, which makes possible performing false lock detection to avoid biased estimates. The PBCH ACF main parameters and scale factors are summarized in Table 2 and in Table 3, respectively.

In conclusion, PBCH-72 compared to PBCH-48 can offer the better estimation accuracy while excluding the largest estimation bias; therefore, since PBCH-72 and PBCH-48 have same transmission rate, we drop the analysis of tracking performance related to PBCH-48.

The PBCHs in a frame are isolated to some extent to each other in terms of the ratio between the ACF maximum and cross-correlation function (CCF) maximum, named isolation factor (ISF) in the following. This allows to exclude signal tracking ambiguity with respect to the PBCHs in a frame. The isolation between the PBCHs in a frame are illustrated in Figure 7 and summarized in Table 4.

Table 2. PBCH ACF main parameters

	Main lobe			First side lobe			Second order main lobe		
	Amp.	Width	Delay	Amp.	Width	Delay	Amp.	With	Delay
PBCH-48	48	562.1 m	0.0 m	10.4	281 m	390.3 m	24	281 m	6651 m
PBCH-72	72	562.1 m	0.0 m	15.6	281 m	390.3 m	-	-	-

Table 3. PBCH ACF scale factors

Main lobe amp. / Second order main lobe amp.	Main lobe amp. / First side lobe amp.	(PBCH-72) Main lobe amp. / (PBCH-48) Main lobe amp.
2.0	4.6	1.5

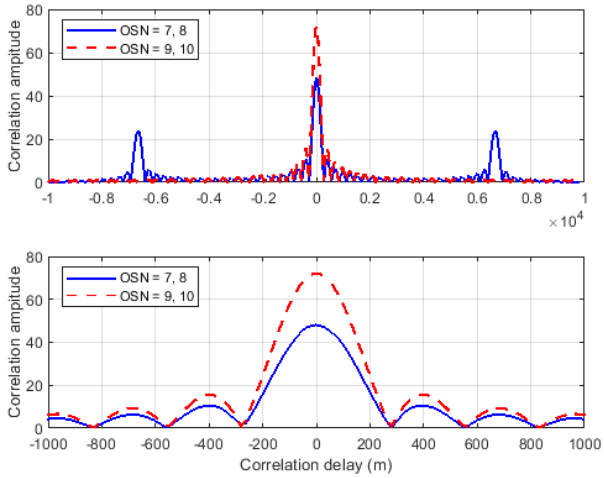

Figure 5. PBCH autocorrelation amplitude as a function of the correlation delay for PBCH in OSN 7-10; (top) zoom out (bottom) zoom in

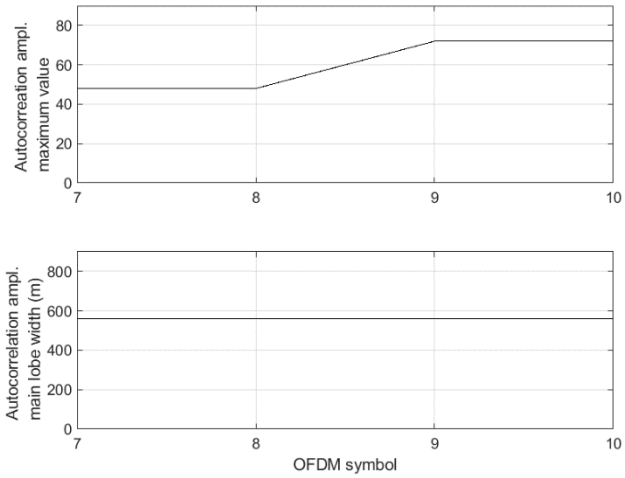

Figure 6. PBCH autocorrelation amplitude (top) maximum (bottom) main lobe width for each sequence in a frame

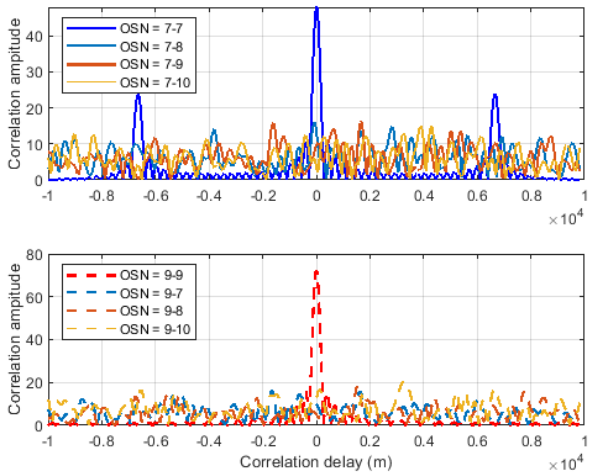

Figure 7. Cross-correlation amplitude of (top) PBCH in OSN 7 with all 4 PBCH in a frame; (bottom) PBCH in OSN 9 with all 4 PBCH in a frame; as a function of the correlation delay

Table 4. Isolation factor between (columns 1-3) PBCH in OSN 7 and PBCH in OSN 8, 9, 10; (columns 4-6) PBCH in OSN 9 and PBCH in OSN 7, 8, 10

ISF 7-8	ISF 7-9	ISF 7-10	ISF 9-7	ISF 9-8	ISF 9-10
3.02	2.97	3.18	4.45	3.95	3.52

PCFICH ACF individual analysis

Figure 8 plots the PCFICH ACF amplitude as a function of the correlation delay for different values of N_{RB}^{DL}. The results show that the width of the main lobe centered at zero delay decreases significantly as the number of resource blocks N_{RB}^{DL} in the LTE signal increases; the results show also that maximum value of central lobe does not change with respect to N_{RB}^{DL}. Therefore, it is expected that the delay error estimate for PCFICH and for a given value of the signal to noise ratio improves significantly as the value of N_{RB}^{DL} increases. The results show, furthermore, the presence of autocorrelation side peaks with non-negligible magnitude. Potentially, this could result in false acquisition or biased tracking worsening the final position solution. In GNSS, similar problems have been faced as new navigation signals using binary offset carrier (BOC) modulation [12, 13] were introduced as part of system modernization. Examples of such signals are GPS M-code, Galileo L1F and Galileo L1P. In this respect, several solutions removing tracking bias threat have been proposed [14-17]. The approach in [13], notably, removes completely the possibility of false lock while affects accuracy minimally. Then, in this paper, it is assumed that the autocorrelation side lobes can be completely removed.

The maximum value and the width of the central lobe of the autocorrelation amplitude for a different number of resource blocks are showed in Figure 9. In sum, the autocorrelation function when reaches its most favorable shape, specifically at the value of resource blocks equal to hundred, it exhibits a central lobe that is as much wide as 562 m and as much high as 16.

Figure 10 plots the PCFICH ACF amplitude as a function of the correlation delay for N_{RB}^{DL} equal to hundred. The results in upper plot show that the central lobe can reliably be approximated as

$$R(u) = A \,\text{sinc}\,(\pi\Delta u)\,\text{rect}\,(0.5\Delta u) \tag{3}$$

where A = 16 and Δ = 0.588. In Equation (3), sinc (·) denotes a sinusoidal cardinalis function [18] and rect (·) denotes a rectangular function. Note that u is expressed in samples which can translate into distance as multiplied by the sampling interval and by the speed of light.

The analytic function for an extended set of values of u in the domain can be defined in early approximation as

$$R'(u) = m(u)\sum_{n=-N/2}^{N/2} g(u-nT) = A\,\text{sinc}\,(\pi\Delta_m u)\sum_{n=-N/2}^{N/2}\text{sinc}\,(\pi\Delta u - nT)\,\text{rect}\,(0.25\Delta(u-nT)) \tag{4}$$

for $|u| < \Delta_m^{-1}$, where the periodic function $g(u) = g(u+nT)$ of period T = 3.4 (i.e., 66.3 m) is modulated by the function $m(u)$, Δ_m = 0.002924 and N = 100.

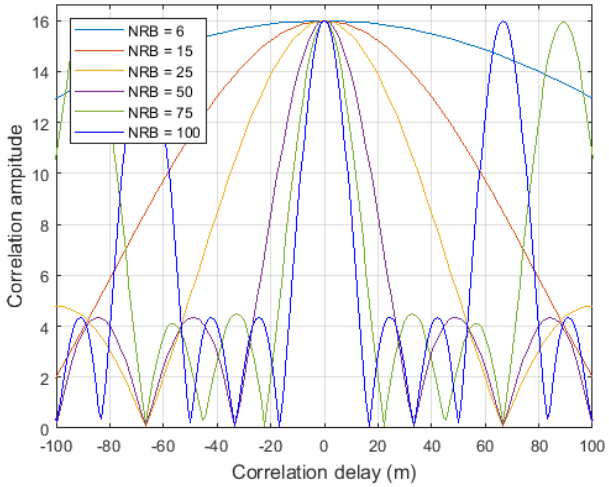

Figure 8. PCFICH autocorrelation amplitude as a function of the correlation delay for a different number of resource blocks. Notation: NRB, total number of downlink resource blocks

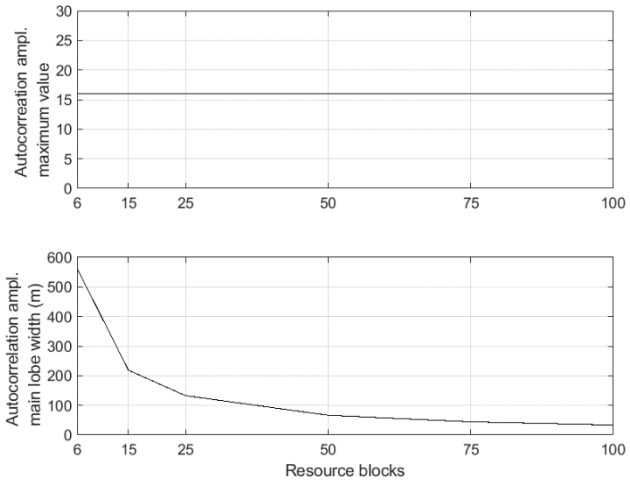

Figure 9. PCFICH autocorrelation amplitude (top) maximum (bottom) main lobe width as a function of N_{RB}^{DL}

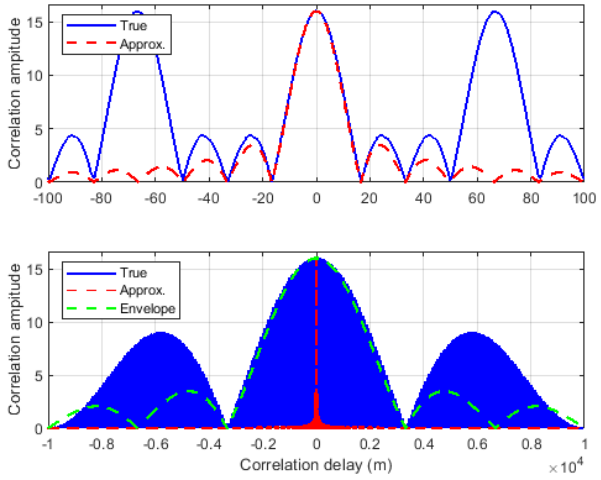

Figure 10. True and approximate PCFICH autocorrelation amplitude as a function of the correlation delay for a number of resource blocks equal to hundred; for (top) small correlation delay and (bottom) large correlation delay

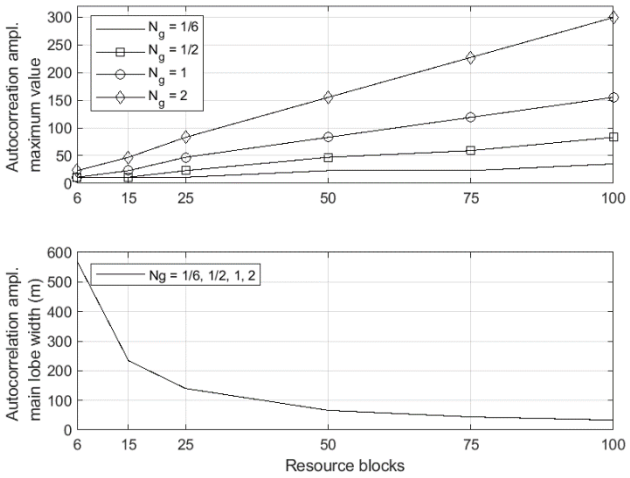

Figure 11. PHICH autocorrelation amplitude (top) maximum (bottom) main lobe width as a function of the number of resource blocks for a different setting of the PHICH resource indicator N_g

PHICH ACF individual analysis

It can be shown that the PHICH ACF amplitude central lobe can be approximated by (3), with the two parameters A and Δ assigned as a function of the system configuration.

Figure 11 shows the maximum value and the width of the PHICH autocorrelation amplitude as a function of the number of resource blocks for a different setting of the PHICH resource indicator N_g. The results show that the amplitude maximum of the central main lobe increases significantly as the number of resource blocks in the LTE signal increases and as the value of the PHICH resource indicator increases; the results show also that the width of the central main lobe decreases significantly as the amount of resource blocks increases, while it is not affected by the value of the PHICH resource indicator. In sum, the autocorrelation function when reaches its most favorable shape, specifically at the value of N_{RB}^{DL} equal to hundred, it exhibits a central lobe that is as much wide as 33 m and as much high as 300.

Finally, based on the results, it is expected that the delay error estimate can significantly improve as a function of both the value of PHICH resource indicator and the number of resource blocks in the LTE signal.

PHYCH ACF comparative analysis

The shape of the autocorrelation amplitude for a set of different physical channels and for the deployment of 20 MHz channel bandwidth is illustrated in Figure 12. The results show that PCFICH, PHICH and CRS have almost the same main lobe width

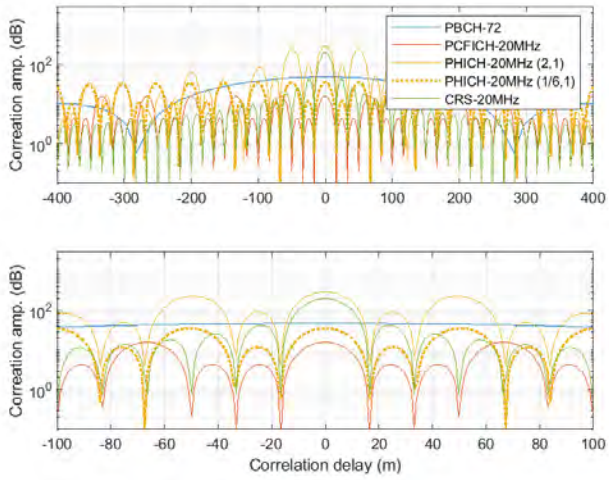

Figure 12. Autocorrelation amplitude as a function of the correlation delay for a set of different physical channels within a common signal of 20 MHz channel bandwidth; (top) zoom out (bottom) zoom in. Notations: PHICH-20MHz (2,1), denotes PHICH for channel bandwidth 20 MHz, for N_g= 2 and for a single orthogonal sequence per PBCH group; PHICH-20MHz (1/6,1), denotes PHICH for channel bandwidth 20 MHz, for N_g= 1/6 and for a single orthogonal sequence per PBCH group

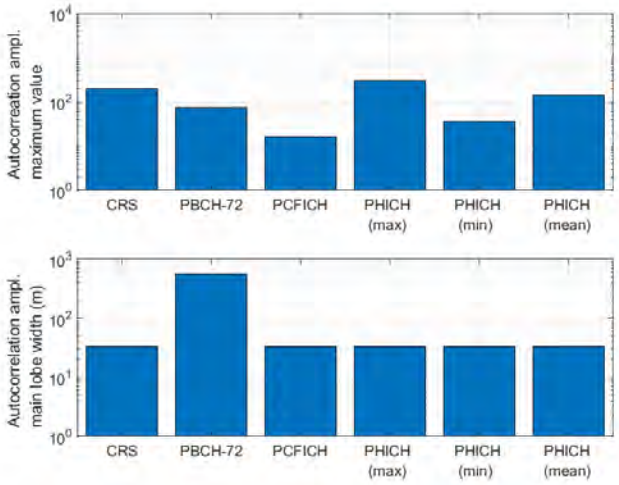

Figure 13. Autocorrelation amplitude (top) maximum (bottom) main lobe width for a set of different physical channels within a common signal of 20 MHz channel bandwidth

but different values of the maximum value of the autocorrelation amplitude. Unlike, PBCH has a much wider main lobe compared the other signals. For PHICH, the autocorrelation amplitude when it reaches its most favorable shape, specifically at the value of N_g equal to two, it exhibits a central lobe that is higher than the central lobe of the autocorrelation amplitude for CRS. The maximum value of the autocorrelation amplitude and the main lobe width for a set of different physical channels and for 20 MHz channel bandwidth are illustrated in Figure 13. Among the analyzed signals, the best shape of the autocorrelation amplitude is represented potentially by PHICH for N_g equal to two.

3.2 Delay tracking error standard deviation

The estimation accuracy of the signal delay can be improved using a delay-looked loop (DLL) which includes, conventionally, a discrimination function and a loop filter.

The first component, often defined as an early-minus-late-power (EMLP) discriminator, once normalized with the derivative of the so-called s-curve in the linear region, produces an error estimate which after filtering is used to update the delay estimate of the next loop input signal. The filter component can reduce the variance of the delay error at the discriminator output by a factor of $2B_lT_l$ [19], where B_l is the one-side loop filter bandwidth expressed in Hertz and T_l is the loop update interval expressed in seconds. The time delay estimate is the variable that can translate to the pseudorange measurement between the emitter and the receiver and that can permit to perform a position computation.

If the total number of pilot data symbols is constant over the estimation time, and if those are uniformly located in the resource elements and have constant and equally distributed power, the standard deviation of the delay error estimate at the loop filter output, expressed in samples, can be written as [8]:

$$\sigma_{\tilde{\varepsilon}} = \sqrt{2B_lT_l \frac{4(1-\operatorname{sinc}\pi\beta\delta)(\operatorname{sinc}\pi\beta\delta/2)^2}{c^2N_p\kappa^2\mathrm{SNR}}\left(1+\frac{(1+\operatorname{sinc}\pi\beta\delta)}{2c^2N_p(\operatorname{sinc}\pi\beta\delta/2)^2\mathrm{SNR}}\right)} \tag{5}$$

whose notation can be summarized as

$\beta = \Delta'_pN_pN_c^{-1}$
Δ'_p is the subcarrier spacing normalized pilot spacing
N_p is the number of pilot subcarriers in the OFDM symbol
N_c is the total number of subcarriers per OFDM symbol
δ is the EMLP correlator spacing [8] expressed in samples
c is the ratio between the amplitude of a pilot subcarrier and the amplitude of a non-pilot subcarrier assumed constant
κ is the normalization factor [8] applied to the DLL discriminator output
SNR is the signal-to-noise ratio defined as the ration between the signal power for N_p pilot subcarriers and the variance of the filtered average white gaussian noise defined as channel additive.

However, the physical channels studied in this paper have data symbols that are not uniformly located in the resource elements of an OFDM symbol. Consequently, for these physical channels the definition $\beta = \Delta'_pN_pN_c^{-1}$ is not valid. To find a parametric expression to relate the opening of the sinus cardinalis function, which arise from the autocorrelation function, to the structure of the physical channels is not easy. Thus, we provide simulation results as follows: β is equal to 0.555 for PBCH-72, 0.588 for PCFICH and PHICH; for N_{RB}^{DL} = 100.

4 SIMULATION RESULTS

In this section, the theoretical performance of physical channel tracking in a noisy single-path environment is evaluated and discussed.

4.1 Simulation setup

The experimental parameters were established using the results in this paper and in [8], as follows: the one side equivalent loop filter bandwidth B_l was set to 20 Hz; the loop update spacing T_l was set to 10 ms for PBCH, 1 ms for PCFICH, 1 ms for PHICH and 0.25 ms for CRS; the correlator spacing δ was set to 1 sample; the parameter β was set to 0.555 for PBCH, 0.588 for PCFICH, 0.588 for PHICH and 0.586 for CRS and the parameter c was set to 1; The number of pilot subcarriers in the OFDM symbol was set to 72 for PBCH, 16 for PCFICH, 300 for PHICH (for N_g = 2), 36 for PHICH (for N_g = 1/6), and 200 for CRS. The sampling frequency F_s was set to 1.92 MHz for PBCH and 30.72 MHz for PCFICH, PHICH and CRS. The experimental results were obtained using Equation (5) and not yet validated with real signal.

4.2 Simulation results

Figure 14 shows the standard deviation of the delay error estimate as a function of the signal to noise ratio for different LTE signals for 20 MHz of system bandwidth.

The results show that the standard deviation of the delay estimate decreases logarithmically with the signal to noise ratio. At SNR 10 dB, the standard deviation of the delay estimate for PBCH-72 is approximately 25.8 cm, for PCFICH-20MHz is approximately 1.0 cm, for PHICH-20MHz (2,1) and PHICH-20MHz (1/6,1) is approximately 0.2 cm and 0.7 cm, respectively; for CRS is approximately 0.1 cm. This is summarized in Table 5 and synthetized as follows

- From PHICH-20MHz (1/6,1) to PHICH-20MHz (2,1) the standard deviation of the delay error estimate is reduced by a factor of 2.9, due to the increase of the number of pilot subcarriers
- The minimum and maximum tracking performance in terms of systematic errors corresponds to PBCH-72 and CRS-20MHz, respectively
- The maximum tracking performance for PHYCH corresponds to PHICH-20MHz (2,1)
- The standard deviation for PHICH-20MHz (2,1) is 4.7 times larger than the standard deviation for CRS-20MHz
- CRS-20MHz outperforms PHICH-20MHz because the decrease in estimation interval associated to the former signal produces more benefit than it does the increase in the number of pilot subcarriers associated to the latter signal.

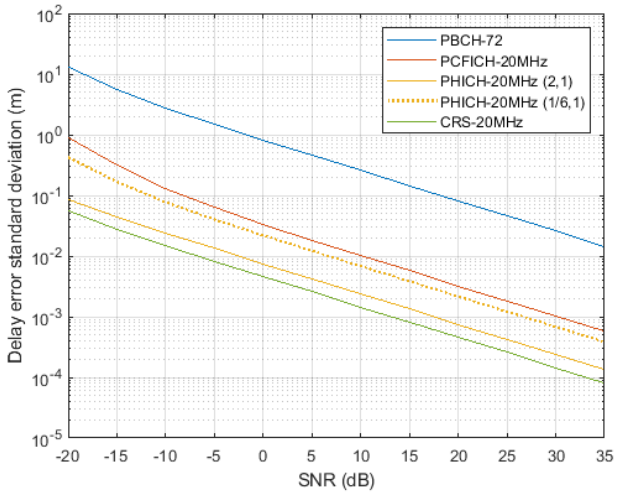

Figure 14. Description of delay tracking errors

Table 5. Standard deviation of delay error estimate $\sigma_{\tilde{\epsilon}}$ for different signals at SNR 10 dB and degradation factor *G* relative to CRS-20MHz

Signal	$\sigma_{\tilde{\epsilon}}$ [cm]	*G*
PBCH-72	25.85	177.7
PCFICH-20MHz	1.02	7.0
PHICH-20MHz (2,1)	0.23	1.6
PHICH-20MHz (1/6,1)	0.68	4.7
CRS-20MHz	0.14	1

5 CONCLUSION

This paper demonstrated that the PBCH, PCFICH and PHICH physical channels in LTE systems can be used for navigation. Firstly, the data symbols carried by these channels must be known and, hence, a correct data symbol detection is demanded. This initial step, which comes before the channel impulse response estimation and the time-of-arrival estimation, however, is not always needed. For instance, the control format indicator, which is carried in PCFICH, is assigned by the network provider using a little set of possible values and therefore is suitable for a brute force searching.

An increased number of available wideband signals with structural diversity can hypothetically be used in either a standalone or a combined fashion to improve the autocorrelation function characteristics and, subsequently, the pseudorange measurement accuracy. Moreover, having such diverse range of signals can lead to different possible acquisition and tracking strategies.

This paper addressed the theoretical tracking performance for different LTE physical channels. Firstly, it is showed that the tracking performance improves as the number of pilot subcarriers increases, and that the number of pilot subcarriers in PHICH

is proportional to the system bandwidth and to the configuration number of PHICH resources. Secondly, it is showed that the tracking performance improves as the transmission bandwidth of the pilots increases, and that the transmission bandwidth of the pilots for PCFICH and PHICH is proportional to the system bandwidth. Thirdly, it is showed that the tracking performance for PBCH is not affected by the system bandwidth. Lastly, the physical channels analyzed in this paper produced a remarkable performance, with PHICH-20MHz (2,1) and CRS-20MHz showing almost the same systematics errors.

AKNOWLEDGMENT
This work has been supported financially by Orolia, which is gratefully acknowledged.

REFERENCES
[1] Tsakiri, M., Kealy A. and Stewart M., "Urban Canyon Vehicle Navigation with Integrated GPS/GLONAS/DR Systems, " *NAVIGATION*, 46(3), 1999, pp. 161-174.
[2] Toledo-Moreo R., Betaille D. and Peyret F., "Lane-level Integrity Provision for Navigation and Map Matching with GNSS, Dead Reckoning, and Enhanced Maps," *IEEE Transactions on Intelligent Transportation System*, 11(1), 2010, pp. 100-112.
[3] McEllroy J., "Navigation Using Signals of Opportunity in the AM Transmission Band," Master's Thesis, Ohio, USA: Air Force Institute of Technology, Wright-Patterson Air Force Base, 2006.
[4] Psiaki M.L. and Slosman B.D., "Tracking of Digital FM OFDM Signals for the Determination of Navigation Observables, " *Proceedings of the 31st International Technical Meeting of the Satellite Division of the Institute of Navigation* (ION GNSS+ 2019), Miami, Florida, September 2019, pp. 2325-2348.
[5] Khalife J. and Kassas Z.M., "Assessment of Differential Carrier Phase Measurements from Orbcomm LEO Satellite Signals for Opportunistic Navigation," *Proceedings of the 31st International Technical Meeting of the Satellite Division of the Institute of Navigation* (ION GNSS+ 2019), Miami, Florida, September 2019, pp. 4053-4063.
[6] Shamaei K. and Kassas Z.M., "LTE Receiver Design and Multipath Analysis for Navigation in Urban Environments," *NAVIGATION*, 65(4), 2018, pp. 655-676.
[7] Thevenon P., Damien S., Julien O. et al., "Positioning Using Mobile TV Based on the DVB-SH Standard," *NAVIGATION*, 58(2), 2011, pp. 71-90.
[8] Soderini A.P., Thevenon P., Macabiau C. et al., "5G-microwave Tracking Performance Characterization," *Proceedings of the 31st International Technical Meeting of the Satellite Division of the Institute of Navigation* (ION GNSS+ 2019), Miami, Florida, September 2019, pp. 2285-2298.
[9] 3GPP, "TS 36.211, Release 15, Technical Specification Group Radio Access Network, Evolved Universal Terrestrial Radio Access (E-UTRA), Physical Channels and Modulation," 2019.
[10] 3GPP, "TS 36.212, Release 15, Technical Specification Group Radio Access Network, Evolved Universal Terrestrial Radio Access (E-UTRA), Multiplexing and Channel Coding," 2019.
[11] 3GPP, "TS 36.331, Release 15, Technical Specification Group Radio Access Network, Evolved Universal Terrestrial Radio Access (E-UTRA), Radio Resource Control, Protocol Specification," 2019.
[12] Betz, J.W., "Binary Offset Carrier Modulations for Radionavigation," *NAVIGATION*, 48(4), 2002, pp. 227-246.
[13] Julien O., Macabiau C., Lachapelle G. et. al., "A New Unambiguous BOC(n,n) Signal Tracking Technique," *Proceeding of the European Navigation Conference*, Rotterdam, The Netherlands, May 2004.
[14] Fine P. and Wilson W., "Tracking Algorithm for GPS Offset Carrier Signals," *Proceedings of the US Institute of Navigation Conference* (ION NTM 1999), San Diego, California, January 1999, pp. 671-676.
[15] Martin N., Leblond V., Guillotel G. et al., "BOC(x,y) Signal Acquisition Techniques and Performances," *Proceedings of the US Institute of Navigation Conference* (ION GPS/GNSS 2003), Portland, Oregon, September 2003, pp. 188-198.
[16] Lin V.S., Dafesh P.A., Wu A. et al., "Study of the Impact of False Lock Points on Subcarrier Modulated Ranging Signals and Recommended Mitigation Approaches," *Proceedings of US Institute of Navigation Annual Meeting* (ION AM 2003), Albuquerque, New Mexico, June 2003, pp. 156-165.
[17] Ward P.W., "A Design Technique to Remove the Correlation Ambiguity in Binary Offset Carrier (BOC) Spread Spectrum Signals," *Proceedings of US Institute of Navigation Annual Meeting* (ION AM 2003), Albuquerque, New Mexico, June 2003, pp. 146-155.
[18] Woodward P.M. and Davies I.L., "Information Theory and Inverse Probability in Telecommunication," *Proceedings of the IEE - Part III: Radio and Communication Engineering*, 99(58), 1952, pp. 37-44.
[19] Betz J.W. and Kolodziejski K.R., "Generalized Theory of Code Tracking with an Early-Late Discriminator Part I: Lower Bound and Coherent Processing," *IEEE Transactions on Aerospace and Electronic Systems*, 45(4), 2009, pp. 1538-1556.